Friction on Small Objects and the Breakdown of Hydrodynamics in Solution: Rotation of Anthracene in Poly(isobutylene) from the Small-Molecule to Polymer Limits

Mikhail I. Sluch, Mark M. Somoza, and Mark A. Berg*

Department of Chemistry and Biochemistry, University of South Carolina, Columbia, South Carolina 29208

Received: January 24, 2002; In Final Form: May 1, 2002

The friction on a nanometer-sized object, as measured by the molecular rotation time of dissolved anthracene, is compared to the macroscopic viscosity in poly(isobutylene) (PIB) over a molecular-weight range extending from the small-molecule limit (isooctane, $M = 114$ g/mol) to the entangled polymer ($M = 85\,000$ g/mol). Calibration studies in small-molecule solvents show that anthracene rotation is a near ideal example of Stokes−Einstein−Debye (SED) behavior with slip boundary conditions. The average rotation time follows SED behavior based on the macroscopic viscosity η_∞ for PIBs up to a moderate length ($M = 615$ g/mol, $\eta_\infty = 2000$ cP). Beyond this length, the rotational friction shows a sharp transition to a weak dependence on the polymer length. The transition length is not associated with any standard length scale of the static polymer structure. In particular, SED behavior continues well beyond the point where the solvent length or volume exceeds the solute's dimensions. An additional transition from exponential to nonexponential rotational relaxation occurs at a shorter polymer length. The breakdown of simple hydrodynamics and the SED model is attributed to exceeding a dynamical length scale associated with torsional flexibility and not to exceeding a simple ratio of solvent-to-solute size.

I. Introduction

Conventionally, the dynamics of polymer melts and of small-molecule liquids are viewed in very different terms. For example, the motions of a solute, either rotational or translational, are typically discussed in relationship to a hydrodynamic model if the solvent molecules are smaller than or similar in size to the solute. In particular, the Stokes−Einstein−Debye (SED) model and its modifications are hydrodynamic models that directly relate the rotation friction on a solute to the macroscopic viscosity of the solvent.[1] In polymer melts, on the other hand, the high diffusivity of small penetrants suggests that macroscopic viscosity might be quite different from the effective friction experienced by a monomer-sized entity.[2−4] This paper bridges the gap between these two regimes by comparing the rotational friction experienced by a small solute with the macroscopic viscosity as the solvent length is changed from the small-molecule limit to the entangled polymer. Specifically, the rotation time of anthracene is compared to viscosity in poly(isobutylene) (PIB) (Figure 1) as a function of chain length from isooctane (molecular weight $M = 114$ g/mol) to the entangled polymer ($M = 85\,000$ g/mol). This paper aims to address the question of what length scale is associated with a change from small-molecule to polymer-like behavior when liquids are viewed on a short length scale. A common view is that the breakdown of hydrodynamics is governed by a simple ratio of the diameters of the solute and solvent. Our results suggest that the ratio of the solvent length to a dynamic torsional correlation length of the solvent is often more important. In the long term, we hope these results on local friction will be useful not only in understanding rotational motion, but also translational diffusion and chemical reactivity in polymer melts and elastomers.

* To whom correspondence should be addressed. Phone: 803-777-1514. Fax: 803-777-1456. E-mail: berg@mail.chem.sc.edu.

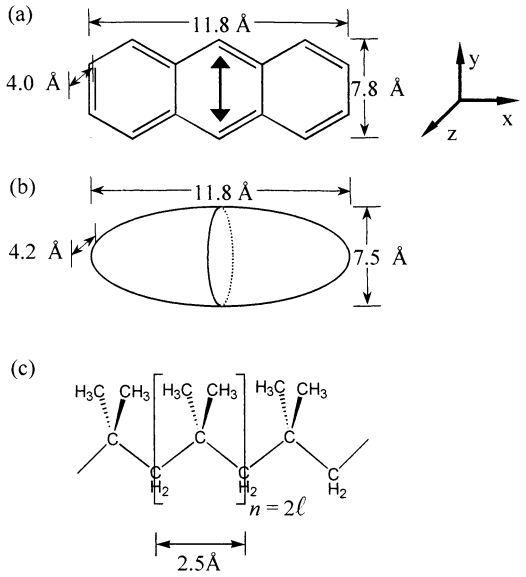

Figure 1. (a) Structure of anthracene showing the axis system used here and the van der Waals dimensions of the molecule.[5] The transition dipole (arrow) for absorption and emission is along the *y*-axis. (b) Dimensions of the effective ellipsoid that reproduces the experimental results (Figure 3) when used in the hydrodynamic rotational diffusion model. The hydrodynamic dimensions are very close to the van der Waals dimensions. Although this ellipsoid is not axially symmetric, it acts as a symmetric rotor under slip boundary conditions. (c) Structure of poly(isobutylene).

The rotation time τ_r of a solute in a small-molecule solvent is usually discussed in reference to the SED equation[1]

$$\tau_r = \frac{\lambda V_h}{kT}\eta_\infty \tag{1}$$

where η_∞ is the macroscopic shear viscosity, T is the temperature

10.1021/jp025549u CCC: $22.00
Published on Web 06/27/2002

and k is the Boltzmann constant. The solute is modeled as an ellipsoid of volume V_h. The axial ratios of the ellipsoid and the boundary conditions determine the shape factor λ.[6−8] Deviations from eq 1 are well-documented for systems with strong electrostatic or hydrogen-bonding interactions[9−28] and for small solutes that rotate without significant solvent displacement.[29−31] However, this equation works quite well for noninteracting solutes in a solvent whose molecules are smaller than the solute,[32,33] if the viscosity is changed by varying the temperature,[34−43] the solvent composition[44] or the pressure.[45−47]

We anticipate that as the solvent molecules become longer and more polymer-like, the local dynamics associated with solute rotation will become disconnected from the macroscopic viscosity. By measuring the rotation time as a function of the solvent length, we will identify the length scale separating the small-molecule and polymer regimes. This information is useful both in identifying the specific mechanisms for the breakdown of hydrodynamic models and for identifying the mechanism causing friction on small-objects and solutes in polymers.

From one perspective, this paper can be regarded as an extension of previous work on rotation in small-molecule solvents to larger solvents. Numerous studies have looked for a breakdown in eq 1 as a result of increasing solvent-molecule size,[32,48−64] most often in series of *n*-alkanes or *n*-alkanols. The interpretation of the *n*-alkanol experiments is complicated because there are large changes in solvent polarity, liquid structure and hydrogen-bonding ability, as well as size, through the series of *n*-alkanols. The *n*-alkane series is less complicated, but is limited to hexadecane and smaller molecules by crystallization of the higher alkanes. The maximum viscosity in *n*-alkane studies is typically ~3.5 cP, and the largest solvent molecules are only slightly larger (by volume) than the solute. Some studies find evidence for deviations from eq 1 in long alkanes and others do not, perhaps due to differences in solute size. In this paper, we will extend the study of solute rotation to much higher viscosity ($\eta_\infty = 5 \times 10^9$ cP) and much larger solvents. As a result, the breakdown of the SED model is much clearer and more dramatic than in previous studies.

From another perspective, this paper can be viewed as an extension of work on local dynamics in polymers. Other experiments, such as neutron scattering[65−70] can look at the short length-scale dynamics of the pure polymer itself. Those experiments look at polymer segmental dynamics, which are related to, but distinct from, the dynamics of a free solute. The dynamics of a free solute studied here depend on both the local polymer dynamics and how the solute couples to those motions.

Many variations of optical anisotropy experiments in polymers have been performed.[71] By covalently bonding the fluorescent label to the polymer, the motion of the polymer itself is observed,[72−76] as in neutron scattering. Of the studies of free solutes, most have not varied the molecular weight of the polymer in a systematic way as this paper does. However, some of these prior studies are in PIB and should be noted.[77−80]

A few previous studies have looked at free-solute rotation as a function of molecular weight in polymers. In a study of four poly(butadiene)s, Fofana et al. attributed the change in rotation time with molecular weight to differences in the glass-transition temperature and in microstructure.[81] Stein et al. looked at five poly(dimethylsiloxane)s (PDMS) in the range $M = 1250-28\,000$ g/mol. They found a very weak dependence of rotation time on molecular weight and rotation times much faster than predicted by eq 1.[74,82] However, a different probe molecule gave different results.[83] Niemeyer and Bright also looked at PDMS in the range $M = 1250-49\,000$ g/mol with different conclusions.[84] They found a strong variation of τ_r with molecular weight and correlated τ_r with bulk density, not viscosity.

In this paper, we look at a common elastomer, poly(isobutylene) (PIB) (Figure 1). Poly(isobutylene) is in widespread commercial use as "butyl rubber" and is notable for having very low diffusivity for solutes, i.e., a high translational friction.[2−4] This study is motivated by the idea that the same mechanisms may be responsible for both translational and rotational friction. In a future paper, we will report comparable measurements on PDMS.[85] PDMS has a static structure very similar to PIBs, but has a very high diffusivity for solutes.[2−4]

After presenting our experimental methods in section II, the rotational behavior of anthracene in small-molecule solvents is studied in section III. These results form a point of reference for the polymer studies in section IV. In particular, we are able to calibrate the rotation time in terms of an effective viscosity at the nanometer length scale. The studies of anthracene rotation vs chain length in PIB are presented in section IV. Several transitions are identified between the small-molecule and high polymer solvents. In section V, we present a scheme to rationalize these results. This interpretations focuses on dynamic flexibility of the solvent molecule as the reason for the breakdown of simple hydrodynamics and the SED model. Section V also compares our results to existing data and theories.

II. Experimental Methods

The macroviscosity of PIB changes by over 10 orders-of-magnitude (0.5 cP − 5×10^9 cP) going from the liquid to the entangled polymer. Because of the wide range of rotation times that results, two different experimental techniques were needed: transient-dichroism for low viscosities and fast rotation times and fluorescence depolarization for high viscosities and slow rotation times.

In transient dichroism experiments, a polarized pump pulse selectively excites those chromophores whose transition dipole are aligned with the pulse's electric field. The sample becomes dichroic, i.e., its absorption of a second pulse of light differs for different polarization directions. The second, probe pulse is polarized at 45° with respect to the pump polarization, so that the dichroism causes a rotation of the probe polarization. The rotation of the polarization is detected as the level of transmission of an analyzing polarizer in the probe beam. As the time between the pump and probe pulses is increased, the solutes rotate, the dichroism decays, and the detected probe intensity decreases.

Our toluene, isooctane, and PDMS data were acquired with a standard transient-dichroism setup[86] that has been described in detail previously.[87] Transient dichroism in the sample was induced and detected by 100 fs frequency doubled pulses from a Ti:sapphire laser tuned to 750 nm. Ninety percent of the 75 mW of 375 nm light was used as the pump beam and the remainder as the probe. A flowing sample was needed to eliminate thermal effects and artifacts from photobyproducts. A free jet was used for most of the transient-dichroism measurements. The sample temperature was kept at 25 °C by circulating the sample through a heat exchanger immediately upstream of the flow jet. A thermistor measured the sample temperature. For the transient dichroism measurements, the time resolution (~100 fs) is high enough that deconvolution of the data is not needed in the fits. An example will be seen later in Figure 5. For isooctane, a free flowing jet was unstable. This sample was vigorously pumped through a fused silica demountable flow cell with a 1 mm path length. A poly(tetrafluoroethylene) insert in the cell narrowed the flow channel and

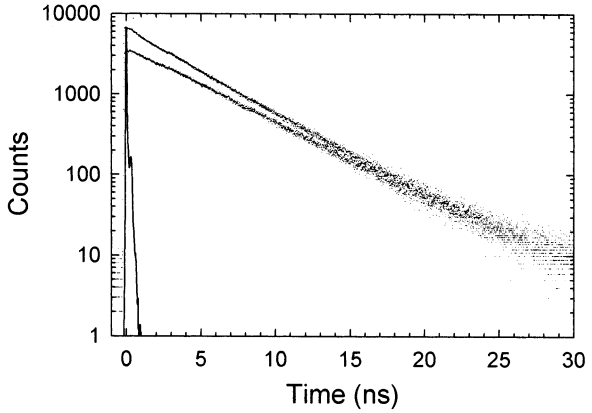

Figure 2. Raw TCSPC data for $M = 750$ g/mol PIB. Upper points: parallel polarization data. Lower points: perpendicular polarization data. Solid line: instrument response function.

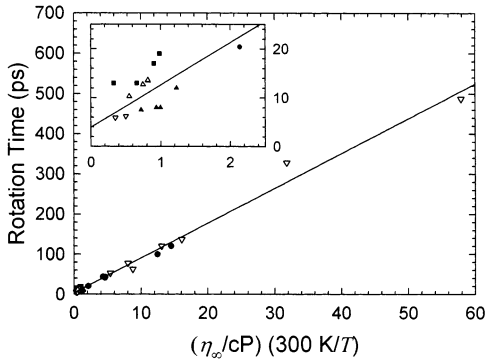

Figure 3. Rotation times τ_r for anthracene in small-molecule solvents versus solvent viscosity. The line is a fit to the modified hydrodynamic model (eq 5, $\tau_0 = 3.95$ ps, slope = 8.68 ps/cP, see Figure 1 for ellipsoid dimensions). (■) − from UV−IR double resonance measurements in CCl_4, C_2Cl_4, C_6D_6, and C_3D_6O by Lettenberger et al.;[94] (▲) − from fluorescence depolarization measurements in cyclohexane by Jas et al.;[5] (△) − from our dichroism experiments in toluene;[97] (●) − from our dichroism experiments in benzyl alcohol;[87] (▽) − from Table 1.

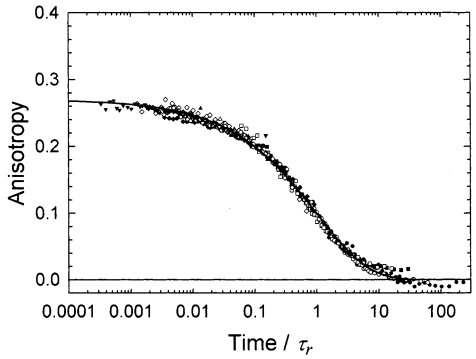

Figure 4. Master plot of anisotropy decays in PIB ($M \geq 350$ g/mol). The time scale for each data set is divided by a scaling time τ_r. The solid curve is stretched exponential fit (eq 6) with $r_0 = 0.27$ and $\beta = 0.52$. Undeconvolved data for real times greater than 50 ps are shown. PIB molecular weights: ○ − 350, ■ − 390, □ − 460, + − 560, ▲ − 680, △ − 750, ◆ − 1290, ◇ − 2500, ▽ − 4400, ▼ − 85 000 g/mol.

increased the flow velocity in the interaction region. The cell was treated with dichlorodimethylsilane to help prevent the accumulation of photodegradation products on the windows. The anthracene concentration was 300 μM, and the absorption at the pump wavelength was 5%. This concentration was much lower than necessary to prevent concentration artifacts, but rather was set low enough to delay accumulation of photodegradation products on the cell windows for the duration of the experiment.

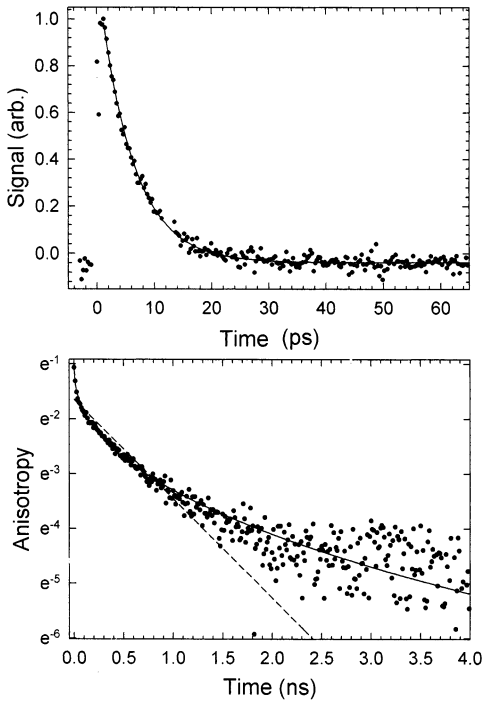

Figure 5. Data bracketing the change from single-exponential to stretched-exponential decay. (a) Dichroism decay of anthracene in isooctane (2,2,4-trimethylpentane). The solid line is a single-exponential fit with decay constant of 5.9 ps. This solvent is small enough to give an exponential decay. (b) Fluorescence depolarization measurement for anthracene in 350 g/mol PIB. A single exponential (dashed) cannot describe the data, whereas the stretched exponential (solid) fits the data very well. The same stretched exponential shape remains for all longer PIBs (see Figure 4).

The dichroism experiment requires a rapidly flowing sample, which is difficult for samples with high viscosity or those that are only available in small quantities. Fortunately, the rotation times in these samples are long and do not require the time resolution of the dichroism experiment. The remainder of the rotational relaxation times were measured by fluorescence depolarization using time-correlated single-photon counting (TCSPC).[88−90] Subpicosecond excitation pulses at 375 nm were generated from a home-built, mode-locked, Ti:sapphire laser with an external acousto-optic pulse selector, followed by second harmonic generation in a 1 mm β-barium borate (BBO) crystal. Fluorescence was collected by a subtractive double monochromator and a Hamamatsu microchannel plate detector. Time-dependent fluorescent decays parallel and perpendicular to the excitation beam were collected for identical times. Anthracene rotation times τ_r were obtained from the anisotropy $r(t)$, which is obtained directly from the time-dependent parallel and perpendicular fluorescence intensities, $I_{||}(t)$ and $I_\perp(t)$

$$r(t) = \frac{I_{||}(t) - I_\perp(t)}{I_{||}(t) + 2I_\perp(t)} \tag{2}$$

To reduce the effects of polarization dependent detection efficiency, a calcite-wedge polarization scrambler was placed at the entrance to the monochromator. The ratio of parallel-to-perpendicular detection efficiency was measured to be 0.96, and this value was used to correct all the data. The typical full width at half-maximum of the instrument response function was 50 ps. Least-squares iterative reconvolution[88,89] was used to deconvolve decay curves with rotation times below 550 ps. Because deconvolution is not compatible with the master-plot

analysis used below, data for longer rotation times was simply truncated below 50 ps, rather than deconvolved. Sample temperature was maintained at 25 °C by thermal contact between the sample cell and an actively regulated sample block. An example of fluorescence depolarization data is shown in Figure 2.

The PIB samples used in these experiments came from several sources. Most of the samples were low polydispersity ($M_W/M_n < 1.1$) standards from PSS Polymer Standards Service ($M =$ 224, 350, 390, 680, 2500, 4400, 15 400 g/mol. The most viscous sample ($M = 85\,000$ g/mol) was from Scientific Polymer Products. The remaining PIBs were from Aldrich ($M =$ 460, 560, 750, 1290 g/mol), as was the isooctane and the probe molecule, anthracene. In all of the cases, the samples were used without further purification. Even thought the purity and polydispersity varied greatly between the polymer standards and the remaining samples, the differences cannot be discerned in the data. Absorption and fluorescence spectra showed no evidence of aggregation in any of the samples. The excited-state lifetime did not vary significantly in the samples, staying within the 5−5.6 ns range.

Macroviscosity data for all but the highest viscosity samples was obtained at 25 °C using Ubbelohde capillary viscometers immersed in a regulated water bath. The macroviscosity of the highest viscosity samples ($M >$ 2500 g/mol) was calculated from temperature-MW-viscosity relationships developed for PIB by Fox and Flory.[91,92]

III. Anthracene Rotation in Small-Molecule Solvents

To use solute rotation to study local friction in polymers, we must have a solute with simple and well understood rotation in small-molecule solvents. In a previous paper, we have shown that anthracene is a nearly ideal example of a hydrodynamic rotor and follows the SED model very well if the solvent molecules are small.[87] Anthracene rotation times also have been measured by several other groups.[93−95] In this section, we review and extend these studies to calibrate anthracene's rotational parameters λ and V_h in the hydrodynamic limit. In small-molecule solvents, anthracene has a single-exponential anisotropy decay, follows the SED equation very well and has the correct initial value of the anisotropy. Section IV will show how each of these properties breaks down as the solvent length increases.

In general, anisotropy decays contain five exponentials.[96] Anthracene's symmetry ensures that the transition dipole moment is along the *y*-axis (Figure 1), reducing the expected number of exponentials to two. However, only one exponential is observed in small-molecule solvents.[87,93,94] In our previous paper, we showed that anthracene's shape causes an accidental degeneracy in the diffusion constants for rotation around the *x*- and *z*-axes, i.e., $D_x = D_z \equiv D_\perp$. In other words, anthracene is a symmetric rotor, even though it has an asymmetric shape. The anisotropy decay reduces to

$$r(t) = r_0\, e^{-t/\tau_r} \tag{3}$$

$$\tau_r = \frac{1}{6D_\perp} \tag{4}$$

where r_0 is the initial anisotropy, the value of the anisotropy extrapolated to zero time. Small deviations from the symmetric-rotor condition may introduce a second exponential, but it is too low in amplitude to be observed.

TABLE 1: New Experimental Data from and Physical Properties of Small-Molecule Solvents

solvent	T (°C)	molecular volume (Å^3)[a]	macro-viscosity (cP)	rotation time (ps)	method[b]
Toluene	−3.9	176	0.74	13.5	DC
	−3.5	176	0.73	13.6	DC
	4.2	176	0.69	12.7	DC
	25.6	176	0.55	10.3	DC
Isooctane	25.0	263	0.35	5.9	DC
PDMS[c]	25.0	354	0.50	6.2	DC
Benzyl Alcohol	1.0	173	12.0	121	FA
	10.0	173	8.3	63	FA
	13.0	173	7.7	78	FA
	25.0	173	5.4	53	FA
Ethylene Glycol	10.0	94	30.0	328	FA
	25.0	94	16.0	137	FA
Cyclohexanol	25.0	175	57.5	488	FA
Anthracene		236			

[a] From densities at 25 °C. [b] FA = Fluorescence anisotropy; DC = Dichroism. [c] $M =$ 162 g/mol.

In Figure 3, the rotation times from single exponential fits in a variety of small-molecule solvents are shown as a function of viscosity. Previously reported values from this lab,[87] from Lettenberger et al.,[94] and from Jas et al.,[95] are shown. New values are reported from TCSPC experiments in benzyl alcohol, ethylene glycol and cyclohexanol, and dichroism experiments in toluene, isooctane and 162 g/mol poly(dimethylsiloxane) (Table 1). All the solvent molecules used in Figure 3 are smaller than anthracene, whether judged on the basis of volume, number of heavy atoms, molecular weight or maximum length.

The small-molecule data follow the modified SED equation[98]

$$\tau_r = \frac{\lambda V_h}{6kT}\eta + \tau_0 \tag{5}$$

very well over a range of viscosities from 0.3 to 60 cP with $\lambda V_h/6kT = 8.68$ ps/cP and $\tau_0 = 3.95$ ps. (The origin of a nonzero τ_0, the rotation time extrapolated to zero viscosity, is poorly understood, but is widely observed.[29,98,99] Because we work primarily with large viscosities, τ_0 has only a small effect on our results.) There is no evidence of "saturation" due to high viscosity itself, if the solvent size remains small. There is also no evidence for a fractional power-law dependence on the viscosity.[1,100] Furthermore, there is no systematic deviation in polar solvents or in hydrogen bonding solvents. There are small solvent-specific deviations from eq 5. Over a small viscosity range, these deviations can obscure the hydrodynamic behavior of the rotation (Figure 3, inset). However, by expanding the range of solvent viscosities measured, the essential hydrodynamic behavior is emphasized. Hydrodynamic rotation is the dominant effect with solvent-specific perturbations superimposed upon it.

The details of anthracene's rotation can be modeled very well as the hydrodynamic rotation of an ellipsoid with slip boundary conditions. (Slip boundary conditions are usually found for medium sized noninteracting solutes such as anthracene.[33,101]) The ellipsoid is defined by the length of the three semiaxes, *a*, *b*, and *c*, as given by the ellipsoid equation, $x^2/a^2 + y^2/b^2 + z^2/c^2 = 1$. The model ellipsoid is found by starting with the lengths of the van der Waals axes (Figure 1a). The axial ratios $b/a = 0.35$ and $c/a = 0.64$ are chosen as the values closest to the van der Waals ratios ($b/a = 0.34$ and $c/a = 0.66$) that also produce a symmetric rotor. These ratios and slip boundary conditions fix the value of the shape parameter $\lambda = 1.12$.[7,8]

Finally, the hydrodynamic volume $V_h = 192$ Å^3 from the fit of eq 5 to the data in Figure 3 is matched to the ellipsoid volume $4abc/3$.

The resulting model ellipsoid is shown in Figure 1b. When used in the hydrodynamic rotational-diffusion model, this ellipsoid reproduces the single-exponential anisotropy decays and the viscosity dependence of the rotation time. Its dimensions ($11.8 \times 7.5 \times 4.2$ Å) are very close to those expected from the van der Waals shape of anthracene ($11.8 \times 7.8 \times 4.0$ Å).

Although the hydrodynamic rotational-diffusion model usually provides the starting point for analyzing solute rotation, it is common to find significant deviations that require excessive adjustment of the model ellipsoid's shape, using the boundary condition as a fitting parameter or introduction of other types of friction. It is also common to find SED-like behavior only if the solvents are restricted to a particular chemical class, e.g., nonpolar or alcohols.[33] Anthracene has none of these problems and is a near ideal example of a hydrodynamic rotor. In part, we attribute this result to a lack of complicating features in the solute: the charge distribution is uniform, so dielectric friction is negligible; there are no hydrogen-bonding sites, so solvent attachment does not occur; the molecular shape is compact and rigid, so modeling by an ellipsoid is accurate. Another factor in finding good agreement with the SED model is that we examine a wide viscosity range, but keep the solvent molecules smaller than the solute.

Anthracene provides an affirmative example of hydrodynamics working well at the molecular level. It suggests that deviations from hydrodynamic behavior in other systems result from the introduction of new effects or violation of the simplifications of the model, rather than an inherent failure of hydrodynamics at the molecular level.

We note that computer simulations of anthracene rotation have seen deviations from SED behavior for the rotational-diffusion constants about individual axes, even when the average diffusion constant seen in experiments does follow SED behavior.[5] If there is a cancellation of errors in the experimental diffusion constant, then the cancellation is quite good under a wide variety of conditions.

In addition to the rotation times, the initial anisotropy r_0 is an important parameter of the rotational motion. The theoretical maximum for r_0 is 0.40, but smaller values are usually observed. We[87] and others[102] have measured a value of $r_0 = 0.34 \pm 0.02$ for anthracene. A low value of r_0 can have several causes: an angle between the absorption and emission dipoles,[21] electronic-state mixing or vibronic coupling.[103] Because anthracene's S_1 state is well separated from other states, and we work near its origin, these mechanisms are not plausible in the current system. In a previous paper,[87] we showed that the missing anisotropy is contained in a subpicosecond, inertial decay component. Simply put, this is the size of a single "step" in the random walk that causes the long diffusive decay. Thus, the magnitude of r_0 is also well understood for anthracene in small-molecule solvents. The next section looks at how these features change in a polymeric solvent.

IV. Anthracene Rotation in Poly(isobutylene)

Nonexponential Decays. The most apparent change in the anisotropy decay in polymeric solvents is that the decays become nonexponential. However, the shape of the nonexponential decay does not change as the polymer increases in size from $M =$ 350 g/mol to 85 000 g/mol. Figure 4 shows a master plot of the anisotropy decays in this range. Each decay has been shifted along the logarithmic time axis to adjust for the change in average rotation time τ_r. The common shape of all the decays becomes apparent.

The common shape is fit by a stretched exponential

$$r(t) = r_0 \exp[-(t/\tau)^{\beta}] \tag{6}$$

with $r_0 = 0.27$ and $\beta = 0.52$. The stretched exponential is a widely used empirical form for describing nonexponential decays.[104] The β parameter describes the degree of nonexponentiality, with $\beta = 1$ corresponding to exponential decay and smaller values corresponding to greater nonexponentiality. The observed value of β is typical of the degree of nonexponentiality found in a wide variety of relaxation processes in viscous fluids, both polymeric and nonpolymeric.[104]

Independent fits of each decay to eq 6 leads to some scatter in the values of r_0 and β, but no systematic trends. Fitting the master plot with eq 6 is equivalent to fitting each individual decay separately with r_0 and β held at their best common values. (The data at 15 400 g/mol had an anomalously high value of r_0, which is attributed to an experimental artifact. This data set is not included in Figure 4.)

The transition from exponential to nonexponential occurs for relatively short chains and over a relatively narrow range of chain lengths. Isooctane (2,2,4-trimethylpentane, $M = 114$ g/mol) can be viewed as a dimer of isobutylene ($\ell = 4$), but it is still smaller than anthracene ($M = 178$ g/mol). It has an exponential anisotropy decay like other small-molecule solvents (Figure 5a). However, by the time the polymer reaches $M =$ 350 g/mol ($\ell = 12$), the decay is clearly nonexponential (Figure 5b). (The decay shape for $M = 224$ g/mol PIB is ambiguous because the fast portion of a stretched exponential would be obscured by the instrument response function.)

The rapid transition from exponential to nonexponential decays followed by a constant decay shape over a wide range of molecular weights and average decay times indicates that the nonexponential shape is not due to the accidental overlap of unrelated processes. If different decay processes were involved, then their decay times should continue to evolve differently with molecular weight, leading to a chain-length dependent decay shape. A model for the onset of nonexponentiality is proposed in section V. Most of the intervening analysis is only concerned with the change of the mean decay time, not with the constant spread around the mean value.

The other important feature of Figure 4 is that the apparent initial anisotropy ($r_0 = 0.27$) is smaller than the value observed in small-molecule solvents ($r_0 = 0.34$). The missing amplitude could represent a fast partial reorientation process unique to polymeric solvents. Other studies are consistent with this proposal. Measurements of r_0 in siloxanes,[82] PIB, polystyrene and polysulfone,[78] and polyisoprene[73] have yielded values around $r_0 = 0.2$. Veissier et al. have reported that r_0 in PIB is dependent on the temperature and solute size, approaching 0.4 for the largest solute.[77] Further experiments at shorter times are needed to clarify the origin of the low value of r_0 in polymers.

SED Rotation in Large-Molecule Solvents. We can now determine if the SED model breaks down when the chain length exceeds the solute size. However, we must first determine how to extract a rotation time characteristic of the nonexponential decays that can be used in eq 5 in place of an exponential time constant. We chose to use the integral average[105]

$$\tau_r = \int_0^{\infty} e^{-(t/\tau)^{\beta}}\, dt = \frac{\tau}{\beta}\Gamma(1/\beta) \tag{7}$$

where $\Gamma(x)$ is the gamma function.[106] In the case of exponential

TABLE 2: Experimental Data from and Physical Properties of Poly(isobutylenes)

molecular weight, M (g/mol)	chain length (ℓ)	anthracene rotation time (ps)[a]	macroviscosity (cP)	nanoviscosity (cP)
114	4	5.9	0.5	0.45
224	8	130	3.2	15
350	12	487	120	55
390	14	1006	190	114
460	16	1.9×10^3	460	210
560	20	7.5×10^3	1.3×10^3	850
680	24	8.5×10^3	5.5×10^3	960
750	27	18×10^3	8.9×10^3	2.0×10^3
1290	46	32×10^3	76×10^3	3.7×10^3
2500	89	44×10^3	540×10^3	5.0×10^3
4400	157	89×10^3	1.2×10^6	10×10^3
15 400	550	1252×10^3	14×10^6	140×10^3
85 000	3036	343×10^3	4.6×10^9	39×10^3

[a] Integral average relaxation times (eq 7) from stretched-exponential fits (single-exponential fit for $M = 114$ g/mol).

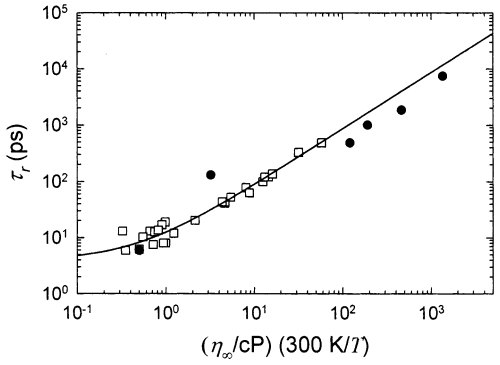

Figure 6. Probe rotation time versus macroviscosity for PIBs (●) and small-molecule solvents (□) in the SED region (114−600 g/mol). The solid line is the SED fit to small-molecule solvents (Figure 3). SED behavior continues for polymer chains significantly longer than anthracene's longest dimension.

decays, this average decay time is the same as the standard exponential decay time. Because this average corresponds to the area under the decay curve, it is relatively robust to the specific functional form used to fit the data. Thus, if a sum of exponentials were used instead of the stretched exponential (eq 6), the area under the experimental points and thus the integral-average time would not change.

The integral average rotation times τ_r for the thirteen PIB samples are collected in Table 2. The molecular weight of the samples ranged from 114 g/mol to 85 000 g/mol, corresponding to a range in bulk viscosities of nearly 10 orders of magnitude (0.5 cP to 4.6×10^9 cP).

Figure 6 compares the integral rotation times for PIBs in the 114−560 g/mol range to the SED behavior found for small-molecule solvents. Although there are deviations due to experimental error and system-specific effects, the overall behavior is dominated by hydrodynamics correlated to the macroviscosity. The basic success of this comparison validates the use of the integral rotation time defined in eq 7 and the neglect of any fast processes leading to the low value of r_0. A systematic over-prediction of the rotation time may be due to the imperfection of these assumptions. However, these imperfections are not important for the purposes of this paper, because the error does not grow systematically with chain length, and the size of the error is small relative to the effects at longer chain length.

This set of solvents that follow SED behavior includes solvent molecules that are clearly larger than the solute. For example, the ratio of volumes of the solvent and solute can be approximated by their molecular-weight ratio. By this measure, the largest solvent molecule following SED behavior is more than three times larger than the solute. In the all-trans configuration, the largest solvent molecule would have a length of 30 Å, about 2.5 times longer than the longest dimension of anthracene. Thus, PIB provides an example that shows that hydrodynamic, SED behavior can occur even if the solute is distinctly smaller than the solvent molecules. The implications of this conclusion are considered further in the discussion.

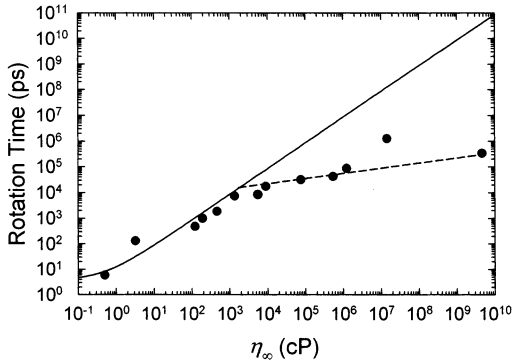

Figure 7. Rotation times for anthracene versus macroviscosity in PIBs of different molecular weights (Table 2). The solid line is the best SED fit for small-molecule solvents (Figure 3). The rotation times follow the SED curve up to moderately long polymers, but deviate for polymers above $M \approx 600$ g/mol (2000 cP). The rotation times continue to increase slowly above this point. The dashed line is an empirical power law fit to the region after the SED model breaks down.

Breakdown of SED Rotation. Although SED behavior persists for unexpectedly long solvent chains, it breaks down for sufficiently long polymers. Figure 7 extends the plot of rotation times to longer polymers ($M = 85\,000$ g/mol, $\ell = 3036$, $\eta_\infty = 4.6 \times 10^9$ cP). The SED line derived from the small-molecule solvents is shown as the solid curve. Over this wider viscosity range, the deviations from SED behavior are dramatic. The breakdown of SED behavior occurs abruptly near a viscosity of 2000 cP, corresponding to a polymer of $M = 600$ g/mol. Deviations from SED behavior become increasingly strong for longer polymers, leading to a greater than five orders-of-magnitude difference between the observed and SED rotation times for the longest polymer.

In the limit of an infinitely long polymer, the macroviscosity will also become infinite. We anticipate that the rotation time will reach a constant value because it should only depend on local properties in the infinite polymer limit. Thus, the rotation time should become independent of the viscosity as the viscosity becomes large.

Figure 7 shows that, despite the abruptness of the breakdown of the SED limit, the rotation time approaches a constant value slowly as the macroviscosity continues to increase. This result suggests that there is another important transformation between the breakdown of the SED model and the infinite polymer limit, but that the second transformation is relatively gradual.

This region can be fit with the formula $\tau_r = 3580$ ps $(\eta_\infty/\text{cP})^{0.2}$. Fractional power laws are often used to fit rotation time vs viscosity data. However, there is little theoretical justification for these fits. We believe that these fits, including ours, are purely empirical. The solvent length, not the viscosity itself, is the correct parameter for discussing the breakdown of macroscopic hydrodynamics. In the next section, the data will be transformed so it can be plotted against the solvent length.

Macro and Nanoviscosity versus Polymer Length. To analyze the PIB data as a function of solvent length, it is useful

to reinterpret the rotation time as defining the viscosity acting on a nanometer-sized object. Inverting eq 5 gives a definition for this "nanoviscosity"

$$\eta_{\mathrm{nm}} = \frac{6kT}{\lambda V_h}(\tau_r - \tau_0) \tag{8}$$

which may be different than the macroviscosity η_∞ acting on a large object.

This definition of a nanoviscosity is not fundamentally different from standard definitions of viscosity. A typical method of measuring viscosity is to solve a well-defined hydrodynamic problem, e.g., the flow time through a cylindrical tube. Once the validity of the hydrodynamic model is verified and calibrated on known samples, the problem is inverted to create an experimental definition of viscosity. In our example, the flow time through a tube becomes a measure of the viscosity on a macroscopic length scale. Similarly, once the SED equation is validated under a variety of conditions, the rotation time of anthracene becomes a measure of the viscosity on a nanometer length scale, through eq 8.

In using the term "nanoviscosity" for our measurements, we leave open the question of how it relates to similar concepts such as "local viscosity", "segmental friction" or "microviscosity". In particular, we recognize that there may be multiple mesoscale viscosities pertinent to different length scales. For example, the viscosity on an object smaller than the chain width (the "angstrom viscosity") or the viscosity acting on a larger object that is still smaller than the entanglement length (the 10-nanometer viscosity) may be different from both the macro- and the nano-viscosities

We want to compare the macro- and nano-viscosities as a function of the size of the solvent molecules. The choice of the appropriate measure of size is important. Because torsional conformations play a key role in our analysis, we use the number of backbone bonds as a measure of polymer size. We define this number in terms of the ratio of the average molecular weight to the molecular weight of the repeat unit of PIB

$$\ell = \frac{2M}{56\mathrm{g/mol}} \tag{9}$$

The factor of 2 reflects the fact that each repeat unit has two backbone bonds. For the shortest polymers, there is an ambiguity in how to treat the ends. Because these issues do not appear to be important in the final analysis, we simply apply eq 9, even for the smallest PIBs. For PIB, ℓ is a trivial rescaling of the molecular weight. However, it is a more robust measure of size for making comparisons to other polymer series, e.g., PDMS or alkanes.[85]

Having chosen appropriate variables, we now replot our data as macro- and nano-viscosities versus polymer length (Figure 8). The macroviscosity itself is a complicated function of the polymer length. We extended the short end of the range of the macroviscosities with the PIB fragments dimethylpropane and 2,2-dimethylbutane.[107] For $\ell < 7$, the macroviscosity is a weak function of solvent length. For longer polymers, the viscosity increases very rapidly with length (approximately as ℓ^5). The increase slows above $\ell \approx 70$. At the critical entanglement length $\ell_c = 600$, the macroviscosity again rises steeply with polymer length.[91,92]

The SED model assumes that the macro- and nano-viscosities are identical. This assumption is true for small PIB fragments. It continues to be true across the transition to a steep length dependence near $\ell = 7$. Thus, this first indication of polymer-like behavior does not cause a breakdown of the SED model. The breakdown of the SED behavior occurs when the macro- and nano-viscosities diverge near $\ell = 22$.

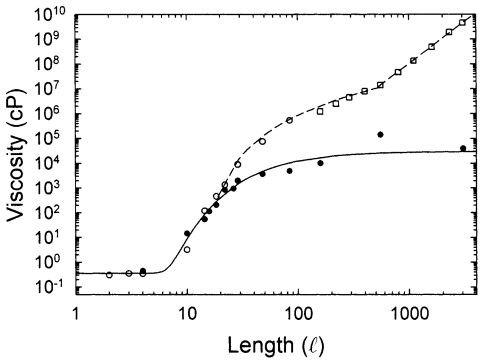

Figure 8. Macro- (open symbols) and nano-viscosity (●) of PIB plotted as a function of chain length ℓ (number of backbone bonds). The macroviscosities of the long polymers (□) are calculated from the viscosity-molecular weight-temperature relationship for PIB of Fox and Flory.[92] The divergence of macro- and nano-viscosities, corresponding to the breakdown of simple hydrodynamics, occurs near $\ell = 22$. The nanoviscosities are fit (solid curve) with eq 10; the macroviscosities (dashed) are fit with eq 12. See also Figure 9.

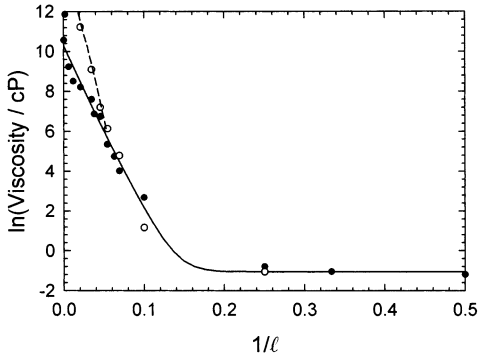

Figure 9. The natural logarithm of the nano- (●) and macro-viscosities (○) of PIB plotted against the inverse of the number of chain atoms in the polymer. The nanoviscosities are fit (solid curve) with eq 10; the macroviscosities (dashed) are fit with eq 12. See also Figure 8.

The nanoviscosity continues to increase with length, but much less rapidly than the macroviscosity. We estimate (see below) that the nanoviscosity in the infinite polymer limit is $\eta_{\mathrm{nm}}^{\infty} = 3.0 \times 10^4$ cP. At the point where the SED behavior breaks down, the nanoviscosity is approximately 1×10^3 cP, a factor of 30 less than the infinite-polymer value. There is a significant increase in the nanoviscosity as the polymer lengthens, even past the point where the macroscopic properties are no longer directly connected to the local properties.

The approach to the infinite-polymer limit is clearer in Figure 9, which plots the logarithm of the viscosity against the inverse of the chain length. On this plot, the data form a straight line as they approach infinite length ($1/\ell = 0$),. Because the density of end groups is proportional to $1/\ell$, this plot implies that the elimination of end effects governs the approach to infinite length. Further discussion is postponed to section V.

The transition from weak to strong dependence on ℓ (near $1/\ell = 0.14$) is also clear on this plot. We have fit the nanoviscosity with the empirical formula

$$\eta_{\mathrm{nm}}(\ell) = \eta_{\mathrm{nm}}^{0} + \eta_{\mathrm{nm}}^{\infty} e^{-A/\ell} \tag{10}$$

to incorporate both the constant and linear regions of Figure 9. The best fit is with $\eta_{\mathrm{nm}}^{0} = 0.35$ cP, $\eta_{\mathrm{nm}}^{\infty} = 3.0 \times 10^4$ cP, and A

$= 90$. (Subscripts refer to solute length; superscripts to polymer length.) The fit is shown in Figures 8 and 9. (The point at $\ell = 550$ is an outlier and is not included in the fit.)

A significant result is that the critical entanglement length has no apparent affect on the nanoviscosity. This result is expected, because the distance between entanglements should be significantly larger than anthracene's dimensions. There should be no need for chains to disentangle to allow a small solute to rotate. However, the breakdown of the SED model is well established before entanglement, and entanglement is not the primary reason for the difference between macro- and nanoviscosity.

Nanoviscosity and Segmental Friction. The Rouse model is a well-known theory for the macroviscosity of polymers below the critical entanglement length.[108−111] The model treats the polymer as a chain of segments, each of which is made up of a number of chain bonds. The connections between segments are completely flexible. The internal details of the segment are not treated, except that each segment experiences a friction due to interaction with the rest of the melt. This model gives the macroviscosity in terms of the polymer length ℓ

$$\eta_\infty(\ell) = \left(\frac{\rho_b L^2 C_\infty}{36}\right)\zeta(\ell)\ell \tag{11}$$

where ζ is the segmental friction coefficient. The leading constants include the density of chain bonds ρ_b and the bond length L. C_∞ is the characteristic ratio of the polymer, a measure of how the real polymer compares to a random walk of a freely jointed model polymer. The most difficult quantity to characterize in this model is the segmental friction coefficient. It has a significant length dependence, which must be modeled before data can be fit.[109,110]

It is tempting to ask if the nanoviscosity measured in our experiments is related to the segmental friction, i.e., if $\eta_{nm} \propto \zeta$. If this is the case we can replace $\zeta(\ell)$ in eq 11 with $\eta_{nm}(\ell)$. We fit the macroviscosity to the modified equation

$$\eta_\infty = D\eta_{nm}(\ell)(\ell - \ell_0) \tag{12}$$

The length independent constants are collected into D. The term ℓ_0 represents the fact that a minimum length is expected before the Rouse model (eq 11) becomes applicable. The fit with $D = 0.85$, $\ell_0 = 17$, and $\eta_{nm}(\ell)$ from eq 10 is shown as a dashed curve in Figures 8 and 9. The agreement with the macroviscosity is quite good.

In general, properties at long times and long length scales, such as the macroviscosity, should be derivable from more fundamental properties at short times and short length scales, like the nanoviscosity. The success of eq 12 shows that the macroviscosity can be derived from the nanoviscosity by using a Rouse-like model and by assuming that the segmental friction of the Rouse model is equal to (or at least proportional to) the nanoviscosity measured in the current experiments. It appears that the nanoviscosity is closely related to the segmental viscosity and that the initial increase of the macroviscosity away from the nanoviscosity is due to a Rouse-like mechanism.

V. Analysis and Discussion

Dynamic vs Static Length Scales. One goal of studying PIB across a broad range of molecular weights was to identify the length scale or scales where transitions from small-molecule to polymer behavior occur, with the hope that these characteristic length scales would help to identify the underlying molecular mechanisms. Table 3 summarizes the transitions seen in our data and compares them to various standard measures of the static structure of PIB and anthracene. The transitions identified in our data are: (1) from weak to strong length dependence of both the macro- and nano-viscosity, (2) from exponential to nonexponential anisotropy decays, (3) the breakdown of SED behavior. As characteristic structural lengths we have taken: (a) the length of the PIB repeat unit (Figure 1), (b) the width of the PIB chain, (c) the characteristic ratio (related to the persistence length of the chain),[113] and (d) the critical entanglement length.[114,115] These sizes are reported both as molecular weights (approximating the chain volume), as the chain length in backbone bonds ℓ (using eq 9 to interconvert between these measures), and the maximum chain length in the all-trans configuration ($2\ell = 2.52$ Å).

TABLE 3: Important Dimensions in PIB and Anthracene

	molecular weight (g/mol)	length[a] backbone bonds (ℓ)	length[a] all-trans (Å)
Anthracene- *x*	178	9.4	11.8[b]
- *y*		6.2	7.8[b]
- *z*		3.2	4.0[b]
PIB repeat unit - length	56	2.0	2.5
- width		5.1	6.4
C_∞[c]	188	6.7	8.4
weak-strong viscosity dependence	196	7	9
exponential-nonexponential	224	8	10
SED breakdown	616	22	28
entanglement[d]	17 000	607	765

[a] 28 g/mol = 1 ℓ = 1.26 Å. [b] Hydrodynamic dimensions. [c] Ref 112. [d] Refs 91 and 92.

The most important transformation is the breakdown of SED behavior. The length associated with this transformation ($\ell = 22$) is not equal to any of the structural lengths in the system. As noted earlier, the PIB length at this transition is substantially longer than any of anthracene's dimensions and shorter than the entanglement length. More significantly, it is three times longer than the length scale determined by the characteristic ratio $C_\infty = 6.7$.[112] C_∞ is the number of backbone bonds needed to make a freely jointed segment that reproduces the end-to-end distance of the PIB chain.[113] Thus, C_∞ can be taken as a measure of the static correlation length of the chain.

At first, it seems that a local property, such as nanoviscosity, could not depend on the chain length once the chain length exceeds the correlation length of the chain. However, our experiments show that the nanoviscosity does not become decoupled from the macroviscosity until a longer length is achieved. We propose that a dynamic correlation length is involved. Within the time of the solute rotation, only a subset of the chain conformations can be sampled. This subset may have a longer correlation length than the full set of conformations contributing to the static correlation length C_∞.

This idea is illustrated more specifically in Figure 10. In the limit of a very long polymer, rotation is fully decoupled from the macroviscosity and occurs through localized motions of the polymer. An example is the crankshaft motion illustrated in Figure 10c. For this motion to occur, there must be torsional barrier crossings at two bonds. These bonds could be relatively close as shown in Figure 10c, or they could be further away from each other. The torsional barriers in PIB are relatively high (4−6 kcal/mol[116]), so on a short time scale, a relatively long length of the polymer needs to be considered before there is a good probability for having this type of concerted torsion within the rotation time. This length defines a dynamic correlation length for the polymer.

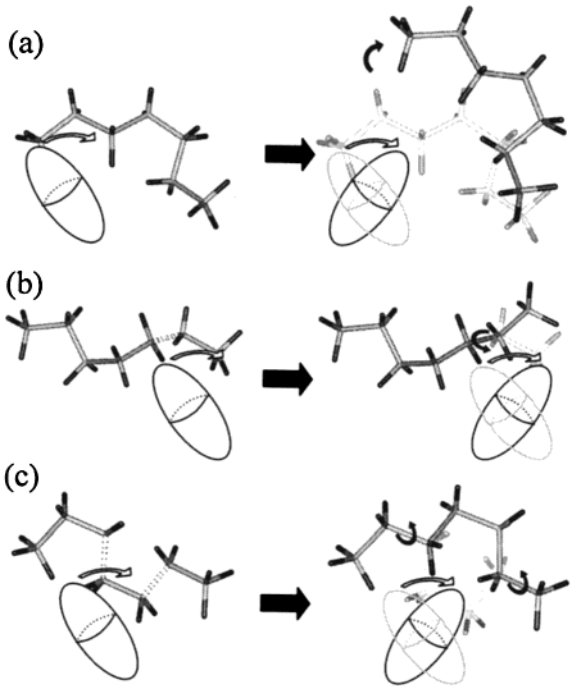

Figure 10. Schematic representation of three types of polymer motion that can accommodate rotation of a small solute (ellipsoid). (a) The polymer can move as a rigid body. This mechanism is most important for short polymers. It accommodates the motion of large and small objects equally well. (b) A single torsional transition (black arrow) can flip a section of the polymer near the end of a chain. (c) Two concerted torsional transitions (black arrows) can cause a crankshaft motion that does not move either end of the chain. (The torsions can also be separated by a larger distance.) This mechanism dominates in the long chain limit. Mechanisms (b) and (c) are much less effective at accommodating the motion of a large object than that of a small one.

When the polymer chain is much longer than this length, the torsional relaxation completely governs the nanoviscosity, and the nanoviscosity is independent of the chain length. The torsional mechanism is ineffective as a direct means of accommodating the motion of a large object. As a result, the macroviscosity is determined by completely different mechanisms (Rouse-like or entanglement) and is much larger than the nanoviscosity.

As the chain length becomes equal to or shorter than the dynamical correlation length, torsional relaxation of a chain during the rotation time becomes less likely, because there are fewer bonds in a given chain. At the same time, rigid-body motions of the short chain (Figure 10a) become more accessible. When the rigid-body motions become more effective in accepting rotational energy than the torsional motions, a transition is seen in the behavior of the nanoviscosity. Short chains respond as a rigid body to both large and small objects and so the macro- and nano-viscosities become equal.

A more precise way to define the dynamic correlation length is to consider a force applied to a single point on a polymer chain at time zero and to measure how far the resulting stress is transmitted along the chain as a function of time. At short times, torsional relaxation has not occurred and the chain responds as a rigid body. Stress occurs along the entire chain length (ignoring propagation effects occurring with the speed of sound on the chain). At slightly longer times and at distant points on the chain, a torsional barrier crossing at an intervening point will relieve the stress. The correlation distance is shortened at this time. As time progresses, this distance shortens further, eventually reaching the static correlation length at long times.

Once the idea of a dynamic correlation length defined by torsional relaxation is accepted as a critical feature of the polymer, the results of our experiments can be rationalized. We outline the resulting explanation in the remainder of the discussion.

Breakdown of Hydrodynamics. The breakdown of hydrodynamics dynamics for molecule-sized objects is a topic of long standing interest in liquid dynamics. The main theories for nonhydrodynamic rotation have been reviewed by Dote, Kivelson, and Schwartz.[117] Their own free-space model illustrates some general features of many of these theories. The free-space model posits that as the solvent molecules become larger, the size of the free space between them increases, causing poorer coupling of the solute rotation to the solvent. Ultimately, the solute becomes a free rotor in the interstitial space between the solvent molecules.

This theory and other existing theories focus on a spherical, or at least compact, solvent molecule, i.e., the solvent molecules have only one characteristic length. The breakdown of hydrodynamics is predicted to occur when the solvent molecular volume exceeds the solute volume. The breakdown is viewed as a problem in coupling between solute and solvent motions. In the large solvent limit, the coupling disappears. For sufficiently large solvents, the rotation times should reach a maximum, turn over and eventually reach the free-rotor time. In this view, the boundary conditions of the hydrodynamic model needs to be modified, not the viscosity.

Many experiments have been aimed at identifying and quantifying the breakdown of hydrodynamics as a function of solvent size.[32,48−64] In accord with the existing theories, most have been interpreted in terms of the ratio of solvent-to-solute size. However, in those experiments, a large range of solvent sizes is not achieved by using large quasi-spherical solvents, but by making longer chains. For example, one of the most popular series consists of the *n*-alkanes from *n*-pentane to *n*-hexadecane. In a chainlike solvent, the solvent-size may greatly exceed the solute size in one dimension, but remain distinctly smaller in the other two dimensions.

Our experiments also use chainlike solvents, but differ from previous studies in two regards. First, we cover a much larger range of lengths than is available in the *n*-alkanes ($5 < \ell < 16$ vs $4 < \ell < 3000$). As a result, we can see the deviations from hydrodynamic behavior becoming very strong (a factor of $>10^5$), whereas previous studies only see the beginnings of a breakdown. We can see quite clearly that for large solvents, the rotation time monotonically approaches a large limiting value. It does not turn over to return to the very fast free-rotor time. The second difference in PIB is that PIB has a greater torsional rigidity than the alkanes, and as a result, PIB's torsional correlation length is longer. This allows SED rotation to continue to much longer chain lengths in PIB.

In our interpretation, the solvent−solute coupling, boundary conditions and the solvent−solute size ratio are not primary features in the breakdown of hydrodynamics, but the solvent torsional rigidity is. If the solvent molecules are torsionally rigid, they absorb energy from both small and large objects in essentially the same way—through rigid-body motions. If the solvent molecules are long enough to be torsionally flexible, a new channel arises for accommodating small-solute motion. Because this channel is not open for large objects, the macro- and nano-viscosities diverge. (Because viscosity is a product of the force initially resisting a motion and the accompanying relaxation time,[118] a faster relaxation causes as a lower viscosity.) Thus, the breakdown of hydrodynamics is determined

primarily by the development of significant intramolecular relaxation mechanisms in the solvent molecules.

We do not claim that the more traditional mechanisms for the breakdown of hydrodynamics do not exist, especially for very small solutes, e.g., N_2 or CO. These effects may account for some of the scatter in our data in the regions that are dominated by SED behavior. However, large compact solvent molecules are not often found in practice, especially if a medium sized solute molecule is considered. In the more common case of chainlike solvent molecules, the mechanism proposed here appears to be the dominant mechanism for the breakdown of hydrodynamics.

Transformation from Small-Molecule to Polymer. A goal of this paper is to gain a better understanding of the transition from a small-molecule liquid to a high-polymer melt. Our data show that this transition occurs in several stages as the polymer lengthens. These transitions can be explained qualitatively as follows.

Transition from Compact to Rigid-Chain. The smallest solvents can be regarded as quasi-spherical or at least as having a compact shape. Rotational motion of the solute requires displacement of solvent molecules. When the solvent is compact, this displacement is accomplished by translation of the center-of-mass of the entire solvent molecule. For a truly spherical solvent, the number of solvent−solvent contacts is invariant to the solvent size. Thus the resistance to center-of-mass motions should not be a strong function of solvent size. In fact, the macroviscosity of the PIB analogues is only weakly dependent on size when the aspect ratio is less than 1.5 ($\ell/ \lesssim 8$).

For longer PIBs ($8 < \ell/ < 22$), both the macro and nanoviscosities increase very rapidly with length. We interpret this region as showing rigid-rod behavior. When the solvent size increases along a single dimension, the number of polymer−polymer contacts increases rapidly. Because the torsional-barrier-crossing rate is low, the polymer still appears rigid on the rotational time scale. The entire solvent molecule must move to accommodate solute rotation, but this type of motion is impeded by the large number of polymer−polymer contacts. Because the polymer is effectively rigid, stress applied at a single point by a small object or along the entire chain by a large object elicits essentially the same result. The macro- and nano-viscosities remain the same. Both the macro- and the nano-viscosity increase rapidly as the polymer lengthens and the number of polymer−polymer contacts increases.

Transition from Torsional Rigidity to Torsional Flexibility. As the polymer length increases further, a point is reached where there is a high probability that a torsional transition will occur somewhere along the chain during the rotation time. These torsional transitions quickly become the dominant mechanism for accommodating the motion of a small solute. However, these transitions cannot accommodate the motion of a large object. Thus, the macroviscosity continues to increase, whereas the nanoviscosity levels off.

Because the polymer is now longer than the static correlation length and because the macroviscosity is measured on a long time scale, the polymer acts as a flexible chain in response to motion of large objects. The increase in macroviscosity is due to a Rouse-like mechanism. From the point of view of the Rouse model, only the longest modes contribute significantly to the macroviscosity, whereas all Rouse-modes plus torsional modes contribute to the nanoviscosity. The macroviscosity increases with length due to the direct linear dependence on length predicted by the Rouse model, on top of a weaker length dependence of the segmental friction. The nanoviscosity gives a good measure of the segmental friction.

Loss of End-Flipping Torsions. On the basis of the discussion so far, the nanoviscosity might be expected to level off quickly after torsional motions become likely. The crankshaft motion shown in Figure 10c is an entirely local torsional motion, whose probability does not increase with increasing chain length. However, the experimental nanoviscosity reaches its long polymer limit rather slowly. Empirically, it reaches that limit as a function of $1/\ell/$ (Figure 9). This finding points to end effects because the density of end groups is proportional to $1/\ell/$.

We suggest that when torsional transitions first become probable, end-group flipping transitions (Figure 10b) are most important in accommodating solute motion. These motions only require a single torsional transition, but that transition must be near a chain end. For an intermediate-length polymer, end-group flipping is the most probable torsional motion of the polymer. As the polymer lengthens, crankshaft motions, which can occur in the middle of the chain, come to dominate (Figure 10c). Because two torsional transitions are required for crankshaft motions, the relaxation becomes slower and the nanoviscosity undergoes a moderate rise.

In our modeling, we have shown a discontinuity in the behavior of the macroviscosity at this transition, but not a discontinuity in the nanoviscosity (Figures 8 and 9). The nanoviscosity undergoes a change in mechanism at this point, and a change in functional form would be expected. However, the change need not be dramatic. For example, in an $\ell/ = 25$ polymer, an end-flip at bond number 20 would be very similar to the rigid-body response of an $\ell/ = 20$ polymer. Thus, we believe that there is a break in the nanoviscosity curve at this transition, but that it is too subtle to be detected with the current data.

Entanglement. At the critical entanglement length, the macroviscosity changes to a much steeper length dependence.[114,115] However, the distance between entanglements is much larger than the dynamic correlation length governing the nanoviscosity. An effect of entanglement on the nanoviscosity is not expected, nor seen.

Transition to Conformational Heterogeneity. Nonexponential relaxations are common in high viscosity media such as polymers and many explanations are possible. For example, mode-coupling effects[119−121] or dynamic heterogeneity associated with the glass transition[122−124] can produce nonexponential decays. However, our samples (300 K) are far from the glass transition temperature ($T_g = 205$ K[110]). Rotational anisotropy can cause multiexponential decays.[102] However, computer simulations show that local anisotropy in polymers is weak far from T_g[125] and is further disrupted by a solute.[126] Furthermore, a similar stretched relaxation ($\beta = 0.55$) is found in PIB by neutron scattering,[65] a technique that should not be affected by rotational anisotropy.

A simple explanation of the sudden onset of nonexponentiality at short polymer lengths is conformational heterogeneity. The transition is close to the length where the aspect ratio, i.e., the ratio of length to width, exceeds 1.5. At this point, the polymer shape is no longer compact, but rather is becoming rodlike. The transition is also close to C_∞, the point where the polymer can exist in a number of different conformations. Once the polymer shape is no longer compact, different conformations will have different shapes and will experience different resistance to moving through the melt. Thus, solute rotation will be faster or slower than the average, depending on the exact conformation of the few polymer chains blocking rotation of the solute. The

distribution of rates causes a nonexponential anisotropy decay. Below the exponential-nonexponential transition, the number of conformations is few, and the effect of the conformation on the overall shape of the polymer molecule is small. The range of rotation rates is narrow, and an exponential anisotropy decay is seen.

Relationship to Other Polymer Studies. A couple of recent studies have also emphasized the idea that a dynamic length scale associated with torsional flexibility is critical in understanding short length-scale dynamics in polymers. A series of papers by Richter et al. has looked at dielectric relaxation, neutron scattering and light scattering in PIB and poly(dimethylsiloxane) (PDMS).[65−69] Deviations from Rouse behavior at large *k*-vectors were seen in PIB, which has high torsional barriers, but not in PDMS, which has low torsional barriers. The deviations define a length scale below which the torsional relaxation in PIB is not fast enough to satisfy the flexibility assumptions of the Rouse model. The length scale for the breakdown of the Rouse model, $k = 0.15$ Å^{-1}, or $\lambda = 40$ Å, is not too different from the length we find for the breakdown of the SED model, 25 Å. The authors of these studies discuss this effect in terms of an internal viscosity due to restricted torsional motion.

Krushev et al. used computer simulations to measure the effects of removing torsional barriers in poly(butadiene).[127] They found that the Rouse model connects the dynamics on the macroscopic length scale with dynamics down to a length scale associated with the wavevector $q = 0.3$ Å$^{-1} = 2\pi/(21$ Å$)$. Thus, they did not see the effects associated with the breakdown of the SED model that we see in PIB, nor the breakdown of the Rouse model seen by Richter et al. in PIB. The reason for the apparent disagreement among these studies is not clear at this time.

Numerous studies of reorientation of optical probe rotation in polymers have been reported. However, most were aimed at different issues and are difficult to compare directly to the current study. Many studies have looked at the fluorescence anisotropy decay of chromophores covalently incorporated into a polymer or oligomer.[72,73,76,77,82,128,129] These studies detect the local polymer dynamics directly, but do not incorporate the issue of coupling between a small molecule and the polymer as the current study does.

A number of studies have looked at solute rotation in polymers as they approach the glass transition.[71,122] Near the glass transition, a number of special issues dominate the dynamics,[78] especially the formation of spatial heterogeneities.[122−124] In this paper, the polymer is well above its glass transition temperature, so the issue of glass transition dynamics is not expected to play a role.

A few studies have looked at free probe rotation as a function of polymer macroviscosity, but vary the viscosity by changing the temperature *T* instead of the molecular weight *M*.[38,79,80,130−132] Often, these studies find that the rotation time is proportional to η_∞/T, as predicted by the SED model, even in long polymers. In our language, this result is expressed as

$$\eta_\infty(T) = f(M)\eta_{nm}(T) \tag{13}$$

Our studies varying *M* at a fixed *T* look at a different aspect of this relationship than studies that vary *T* at fixed *M*. The results of the two types of study are compatible if the factorization in eq 13 is assumed. This hypothesis could be more rigorously tested by studies varying both *M* and *T* in a single system.

The most relevant previous studies are those of solute rotation in poly(dimethylsiloxane) (PDMS). PDMS is structurally very similar to PIB, but has much lower torsional barriers. In our scheme, the transition to dynamic flexibility should occur for much shorter chains. Stein et al. measured rotation times of a polar solute in PDMS at several molecular weights and found a nanoviscosity (in our terminology) much lower than the macroviscosity and only weakly dependent on chain size.[82] However, later studies by the same group suggested that the dipole moment of the solute was complicating the interpretation, i.e., it experienced strong dielectric friction.[83] Niemeyer and Bright used a very large solute to measure rotation times as a function of polymer molecular weight in PDMS.[84] They also sited the importance of end effects in determining the approach to the long polymer limit. However, their probe was not calibrated in small-molecule solvents. Although qualitatively deviations from SED behavior are apparent, a direct comparison of macro- and nano-viscosities was not possible.

In view of the unresolved questions in PDMS, we have undertaken a study of anthracene in PDMS for direct comparison to the PIB results given here. The results will be published in full soon.[85] In brief, the nanoviscosity behaves qualitatively differently in PDMS than in PIB, despite the structural similarities of the two polymers. In particular, the static correlation lengths are nearly the same.[68,112,133] PDMS does not have the region we associate with an extended rigid body. It goes directly from compact to flexible behavior. This result is consistent with the importance of dynamical correlation length determined by torsional transitions.

VI. Conclusions

The friction acting on the rotation of a nanometer sized solute has been compared to the viscosity experienced by a large object over a broad range of solvent chain lengths. The breakdown of a simple hydrodynamic description of the liquid, as in the Stokes−Einstein−Debye (SED) model, is clearly observed. Many previous discussions have emphasized the ratio of solvent and solute diameters in the breakdown of hydrodynamics in liquids consisting of quasispherical molecules. We find that for chainlike solvent molecules, the SED model can extend to solvents that consist of molecules significantly longer than the solute, if the solvent molecules remain rigid on the time scale of the rotation. We suggest that in chainlike solvents, the breakdown of simple hydrodynamic models is governed by a dynamical correlation length related to the torsional conformations of the chain.

These studies have bridged the typical regimes of small-molecule and polymeric solvents. In terms of small-solute dynamics, the transition does not occur in a single step. Rather it involves three distinct effects, which can change at different lengths: (1) a change from a compact to an extended rodlike shape; (2) a change from a dynamically rigid to dynamically flexible rod; and (3) the loss of end effects. In our interpretation, the length scale of (2) is determined by the height of the torsional barriers of the polymer. A future publication will compare the results presented here for PIB with similar results for PDMS, a polymer with similar structure, but very different torsional barriers.[85]

Acknowledgment. This work was supported by the Office of Naval Research through the University Research Initiative Grant No. N00014-97-1-0806.

References and Notes

(1) Fleming, G. R. *Chemical Applications of Ultrafast Spectroscopy*; Oxford University Press: Oxford, 1986.

(2) van Amerongen, G. J. *Rubber Chem. Technol.* **1964**, *37*, 1065.
(3) *Diffusion in Polymers*; Crank, J.; Park, G. S., Eds.; Academic Press: London, 1968.
(4) Vieth, W. R. *Diffusion in and Through Polymers*; Hanser Publishers: Munich, 1991.
(5) Jas, G. S.; Wang, Y.; Pauls, S. W.; Johnson, C. K.; Kuczera, K. *J. Chem. Phys.* **1997**, *107*, 8800.
(6) Hu, C.; Zwanzig, R. *J. Chem. Phys.* **1974**, *60*, 4354.
(7) Youngren, G. K.; Acrivos, A. *J. Chem. Phys.* **1975**, *63*, 3846.
(8) Sension, R. J.; Hochstrasser, R. M. *J. Chem. Phys.* **1992**, *98*, 2490.
(9) Alavi, D. S.; Hartman, R. S.; Waldeck, S. H. *J. Chem. Phys.* **1991**, *94*, 4509.
(10) Hartman, R. S.; Waldeck, D. H. *J. Phys. Chem.* **1994**, *98*, 1386.
(11) Kurnikova, M. G.; Waldeck, D. H.; Coalson, R. D. *J. Chem. Phys.* **1996**, *105*, 628.
(12) Balabai, N.; Sukharevsky, A.; Read, I.; Strazisar, B.; Kurnikova, M.; Hartman, R. S.; Coalson, R. D.; Waldeck, D. H. *J. Mol. Liq.* **1998**, *77*, 37.
(13) Kurnikova, M. G.; Balabai, N.; Waldeck, D. H.; Coalson, R. D. *J. Am. Chem. Soc.* **1998**, *120*, 6121.
(14) Hartman, R. S.; Konitsky, W. M.; Waldeck, D. H.; Chang, Y. J.; Castner, E. W. *J. Chem. Phys.* **1997**, *106*, 7920.
(15) Kumar, P. V.; Maroncelli, M. *J. Chem. Phys.* **2000**, *112*, 5370.
(16) Horng, M. L.; Gardecki, J. A.; Maroncelli, M. *J. Phys. Chem. A* **1997**, *101*, 1030.
(17) Maroncelli, M. *J. Chem. Phys.* **1997**, *106*, 1545.
(18) Papazyan, A.; Maroncelli, M. *J. Chem. Phys.* **1995**, *102*, 2888.
(19) Moog, R. S.; Bankert, D. L.; Maroncelli, M. *J. Phys. Chem.* **1993**, *97*, 1496.
(20) Dutt, G. B.; Singh, M. K.; Sapre, A. V. *J. Chem. Phys.* **1998**, *109*, 5994.
(21) Dutt, G. B.; Srivatsavoy, V. J. P.; Sapre, A. V. *J. Chem. Phys.* **1999**, *110*, 9623.
(22) Dutt, G. B.; Krishna, G. R. *J. Chem. Phys.* **2000**, *112*, 4676.
(23) Dutt, G. B. *J. Chem. Phys.* **2000**, *113*, 11 154.
(24) Dutt, G. B.; Raman, S. *J. Chem. Phys.* **2001**, *114*, 6702.
(25) Dutt, G. B.; Krishna, G. R.; Raman, S. *J. Chem. Phys.* **2001**, *115*, 4732.
(26) Dutt, G. B.; Ghanty, T. K.; Singh, M. K. *J. Chem. Phys.* **2001**, *115*, 10 845.
(27) Srivastava, A.; Doraiswamy, S. *J. Chem. Phys.* **1995**, *103*, 6197.
(28) Imeshev, G.; Khundkar, L. R. *J. Chem. Phys.* **1995**, *103*, 8322.
(29) Bauer, D. R.; Alms, G. R.; Brauman, J. I.; Pecora, R. *J. Chem. Phys.* **1974**, *61*, 2255.
(30) Pereira, M. A.; Share, P. E.; Sarisky, M. J.; Hochstrasser, R. M. *J. Chem. Phys.* **1991**, *94*, 2513.
(31) Irwin, A. D.; Assink, R. A.; Henderson, C. C.; Cahill, P. A. *J. Phys. Chem.* **1994**, *98*, 11 832.
(32) Ben-Amotz, D.; Drake, J. M. *J. Chem. Phys.* **1988**, *89*, 1019.
(33) Williams, A. M.; Jiang, Y.; Ben-Amotz, D. *Chem. Phys.* **1994**, *180*, 119.
(34) Lombardi, J. R.; Raymonda, J. W.; Albrecht, A. C. *J. Chem. Phys.* **1964**, *40*, 1148.
(35) Barkley, M. D.; Kowalczyk, A. A.; Brand, L. *J. Chem. Phys.* **1981**, *75*, 3581.
(36) Canonica, S.; Schmid, A. A.; Wild, U. P. *Chem. Phys. Lett.* **1985**, *122*, 529.
(37) Viovy, J. L. *J. Phys. Chem.* **1985**, *89*, 5465.
(38) Blackburn, F. R.; Cicerone, M. T.; Ediger, M. D. *J. Polym. Sci. Pt. B−Polym. Phys.* **1994**, *32*, 2595.
(39) Blackburn, F. R.; Wang, C. Y.; Ediger, M. D. *J. Phys. Chem.* **1996**, *100*, 18 249.
(40) Brocklehurst, B.; Young, R. N. *J. Phys. Chem.* **1995**, *99*, 40.
(41) Brocklehurst, B.; Young, R. N. *J. Phys. Chem. A* **1999**, *103*, 3809.
(42) Brocklehurst, B.; Young, R. N. *J. Phys. Chem. A* **1999**, *103*, 3818.
(43) Dutt, G. B.; Srivatsavoy, V. J. P.; Sapre, A. V. *J. Chem. Phys.* **1999**, *111*, 9705.
(44) Megens, M.; Sprik, R.; Wegdam, G. H.; Lagendijk, A. *J. Chem. Phys.* **1997**, *107*, 493.
(45) Artaki, I.; Jonas, J. *J. Chem. Phys.* **1985**, *82*, 3360.
(46) Schroeder, J.; Schwarzer, D.; Troe, J. *Ber. Bunsen-Ges. Phys. Chem. Chem. Phys.* **1990**, *94*, 1249.
(47) Ito, N.; Kajimoto, O.; Hara, K. *Chem. Phys. Lett.* **2000**, *318*, 118.
(48) Philips, L. A.; Webb, S. P.; Clark, J. H. *J. Chem. Phys.* **1985**, *83*, 5810.
(49) Lee, M.; Bain, A. J.; McCarthy, P. J.; Han, C. H.; Haseltine, J. N.; Smith III, A. B.; Hochstrasser, R. M. *J. Chem. Phys.* **1986**, *85*, 4341.
(50) Ben-Amotz, D.; Scott, T. W. *J. Chem. Phys.* **1987**, *87*, 3739.
(51) Courtney, S. H.; Kim, S. K.; Canonica, S.; Fleming, G. R. *J. Chem. Soc. Far. Trans. 2* **1986**, *82*, 2065.
(52) Kim, S. K.; Fleming, G. R. *J. Phys. Chem.* **1988**, *92*, 2168.
(53) Bowman, R. M.; Eisenthal, K. B. *Chem. Phys. Lett.* **1989**, *155*, 99.
(54) Roy, M.; Doraiswamy, S. *J. Chem. Phys.* **1993**, *98*, 3213.
(55) Jiang, Y.; Blanchard, G. J. *J. Phys. Chem.* **1994**, *98*, 6436.
(56) Jiang, Y.; Blanchard, G. J. *J. Phys. Chem.* **1995**, *99*, 7904.
(57) De Backer, S.; Dutt, G. B.; Ameloot, M.; DeSchryver, F. C.; Müllen, K.; Holtrup, F. *J. Phys. Chem.* **1996**, *100*, 512.
(58) Benzler, J.; Luther, K. *Chem. Phys. Lett.* **1997**, *279*, 333.
(59) Pauls, S. W.; Hedstrom, J. F.; Johnson, C. K. *Chem. Phys.* **1998**, *237*, 205.
(60) Singh, M. K. *Photochem. Photobiol.* **2000**, *72*, 438.
(61) Rice, S. A.; Kenney-Wallace, G. A. *Chem. Phys.* **1980**, *47*, 161.
(62) Wirth, M. J.; Chou, S. H. *J. Phys. Chem.* **1991**, *95*, 1786.
(63) Kim, Y. R.; Hochstrasser, R. M. *J. Phys. Chem.* **1992**, *96*, 9595.
(64) Anderton, R. M.; Kauffman, J. F. *J. Phys. Chem.* **1994**, *98*, 12 117.
(65) Richter, D.; Arbe, A.; Colmenero, J.; Monkenbusch, M.; Farago, B.; Faust, R. *Macromolecules* **1998**, *31*, 1133.
(66) Richter, D.; Monkenbusch, M.; Allgeier, J.; Arbe, A.; Colmenero, J.; Farago, B.; Bae, Y. C.; Faust, R. *J. Chem. Phys.* **1999**, *111*, 6107.
(67) Harnau, L. *J. Chem. Phys.* **2000**, *113*, 11 396.
(68) Richter, D.; Monkenbusch, M.; Pykhout-Hintzen, W.; Arbe, A.; Colmenero, J. *J. Chem. Phys.* **2000**, *113*, 11 398.
(69) Arbe, A.; Monkenbusch, M.; Stellbrink, J.; Richter, D.; Farago, B.; Almdal, K.; Faust, R. *Macromolecules* **2001**, *34*, 1281.
(70) Smith, G. D.; Paul, W.; Monkenbusch, M.; Richter, D. *J. Chem. Phys.* **2001**, *114*, 4285.
(71) Ediger, M. D. *Annu. Rev. Phys. Chem.* **1991**, *42*, 225.
(72) Viovy, J. L.; Monnerie, L.; Merola, F. *Macromolecules* **1985**, *18*, 1130.
(73) Hyde, P. D.; Ediger, M. D.; Kitano, T.; Ito, K. *Macromolecules* **1989**, *22*, 2253.
(74) Stein, A. D.; Hoffman, D. A.; Frank, C. W.; Fayer, M. D. *J. Chem. Phys.* **1992**, *96*, 3269.
(75) Leezenberg, P. B.; Fayer, M. D.; Frank, C. W. *Pure Appl. Chem.* **1996**, *68*, 1381.
(76) Leezenberg, P. B.; Marcus, A. H.; Frank, C. W.; Fayer, M. D. *J. Phys. Chem.* **1996**, *100*, 7646.
(77) Veissier, V.; Viovy, J. L.; Monnerie, L. *J. Phys. Chem.* **1989**, *93*, 1709.
(78) Inoue, T.; Cicerone, M. T.; Ediger, M. D. *Macromolecules* **1995**, *28*, 3425.
(79) Ediger, M. D.; Inoue, T.; Cicerone, M. T.; Blackburn, F. R. *Macromol. Symp.* **1996**, *101*, 139.
(80) Bainbridge, D.; Ediger, M. D. *Rheol. Acta* **1997**, *36*, 209.
(81) Fofana, M.; Veissier, V.; Viovy, J. L.; Monnerie, L. *Polymer* **1989**, *30*, 51.
(82) Stein, A. D.; Hoffmann, D. A.; Marcus, A. H.; Leezenberg, P. B.; Frank, C. W.; Fayer, M. D. *J. Phys. Chem.* **1992**, *96*, 5255.
(83) Diachun, N. A.; Marcus, A. H.; Hussey, D. M.; Fayer, M. D. *J. Am. Chem. Soc.* **1994**, *116*, 1027.
(84) Niemeyer, E. D.; Bright, F. V. *Macromolecules* **1998**, *31*, 77.
(85) Somoza, M. M.; Sluch, M. I.; Berg, M. A. *Macromolecules*, in preparation.
(86) Alvari, D. S.; Harman, R. S.; Waldeck, D. H. *J. Chem. Phys.* **1990**, *92*, 4055.
(87) Zhang, Y.; Sluch, M. I.; Somoza, M. M.; Berg, M. A. *J. Chem. Phys.* **2001**, *115*, 4212.
(88) Holtom, G. R. "Artifacts and Diagnostics in Fast Fluorescence Measurements"; Time-Resolved Laser Spectroscopy in Biochemistry II, 1990.
(89) Birch, D. S.; Imhof, R. E. Time-Domain Fluorescence Spectroscopy Using Time-Correlated Single-Photon Counting. In *Topics in Fluorescence Spectroscopy, Volume 1: Techniques*; Lakowicz, J. R., Ed.; Plenum Press: New York, 1991; p 1.
(90) Small, E. W. Laser Sources and Microchannel Plate Detectors for Pulse Fluorometry. In *Topics in Fluorescence Spectroscopy, Volume 1: Techniques*; Lakowicz, J. R., Ed.; Plenum Press: New York, 1991; p 97.
(91) Fox, T. G.; Flory, P. J. *J. Am. Chem. Soc.* **1948**, *70*, 2384.
(92) Fox, T. G.; Flory, P. J. *J. Phys. Chem.* **1951**, *55*, 221.
(93) Dorfmüller, T.; Daum, B.; Hanschmidt, A. *J. Chem. Phys.* **1991**, *95*, 813.
(94) Lettenberger, M.; Emmerling, F.; Gottfried, N. H.; Laubereau, A. *Chem. Phys. Lett.* **1995**, *240*, 324.
(95) Jas, G. S.; Kuczera, K. *Chem. Phys.* **1997**, *214*, 229.
(96) Tao, T. *Biopolymers* **1969**, *8*, 609.
(97) Zhang, Y.; Berg, M. A., in preparation.
(98) Alms, G. R.; Bauer, D. R.; Brauman, J. I.; Pecora, R. *J. Chem. Phys.* **1973**, *58*, 5570.
(99) Evans, G. T.; Kivelson, D. *J. Chem. Phys.* **1986**, *84*, 385.
(100) Zwanzig, R.; Harrison, A. K. *J. Chem. Phys.* **1985**, *83*, 5861.
(101) Ravi, R.; Ben-Amotz, D. *Chem. Phys.* **1994**, *183*, 385.
(102) Hyde, P. D.; Ediger, M. D. *J. Chem. Phys.* **1990**, *92*, 1036.
(103) Albrecht, A. C. *J. Mol. Spectrosc.* **1961**, *6*, 84.
(104) *Disorder Effects on Relaxational Processes: Glasses, Polymers, Proteins*; Richert, R., Blumen, A., Eds.; Springer: Berlin, 1994.
(105) Lindsey, C. P.; Patterson, G. D. *J. Chem. Phys.* **1980**, *73*, 3348.

(106) *Handbook of Mathematical Functions*; Abramowitz, M.; Stegun, I. A., Eds.; Dover Publications: New York, 1965.
(107) *Lange's Handbook of Chemistry*, 13th ed.; Dean, J. A., Ed.; McGraw-Hill: New York, 1985.
(108) Ferry, J. D.; Landel, R. F.; Williams, M. L. *J. Appl. Phys.* **1955**, *26*, 359.
(109) Berry, G. C.; Fox, T. G. *Adv. Polymer Sci.* **1968**, *5*, 261.
(110) Ferry, J. D. *Viscoelastic Properties of Polymers*, 3rd ed.; John Wiley & Sons: New York, 1980.
(111) Doi, M.; Edwards, S. F. *The Theory of Polymer Dynamics*; Clarendon Press: Oxford, 1986.
(112) Suter, U. W.; Saiz, E.; Flory, P. J. *Macromolecules* **1983**, *16*, 1317.
(113) Flory, P. J. *Statistical Mechanics of Chain Molecules*; Hanser Publishers: Munich, 1989.
(114) Fox, T. G.; Loshaek, S. *J. Appl. Phys.* **1955**, *26*, 1080.
(115) Markovitz, H.; Fox, T. G.; Ferry, J. D. *J. Phys. Chem.* **1962**, *66*, 1567.
(116) Batie, R. D. d. l.; Laurpêtre, F.; Monnerie, L. *Macromolecules* **1989**, *22*, 2617.
(117) Dote, J. L.; Kivelson, D.; Schwartz, R. N. *J. Phys. Chem.* **1981**, *85*, 2169.
(118) Tschoegl, N. W. *The Phenomenological Theory of Linear Viscoelastic Behavior*; Springer: Berlin, 1989.
(119) Götze, W. Aspects of Structural Glass Transitions. In *Liquids, Freezing and the Glass Transition*; Hansen, J. P., Levesque, D., Zinn-Justin, J., Eds.; Elsevier Science: Amsterdam, 1991; p 289.
(120) Götze, W.; Sjögren, L. *Rep. Prog. Phys.* **1992**, *55*, 241.
(121) Götze, W.; Sjögren, L. *Transp. Theory Stat. Phys.* **1995**, *24*, 801.
(122) Ediger, M. D. *Annu. Rev. Phys. Chem.* **2000**, *51*, 99.
(123) Sillescu, H. *J. Non-Cryst. Solids* **1999**, *243*, 81.
(124) Glotzer, S. C. *J. Non-Cryst. Solids* **2000**, *274*, 342.
(125) Rigby, D.; Roe, R.-J. *J. Chem. Phys.* **1988**, *89*, 5281.
(126) Chassapis, C. S.; Petrou, J. K.; Petropoulos, J. H.; Theodorou, D. N. *Macromolecules* **1996**, *29*, 3615.
(127) Krushev, S.; Paul, W.; Smith, G. D. *Macromolecules* **2002**, *35*, 4198.
(128) Viovy, J. L.; Frank, C. W.; Monnerie, L. *Macromolecules* **1985**, *18*, 2606.
(129) Soutar, I.; Swanson, L.; Christensen, R. L.; Drake, R. C.; Phillips, D. *Macromolecules* **1996**, *29*, 4931.
(130) Hyde, P. D.; Ediger, M. D. *Macromolecules* **1989**, *22*, 1510.
(131) Wang, C. Y.; Ediger, M. D. *Macromolecules* **1997**, *30*, 4770.
(132) Hall, D. B.; Deppe, D. D.; Hamilton, K. E.; Dhinojwala, A.; Torkelson, J. M. *J. Non-Cryst. Solids* **1998**, *235*−*237*, 48.
(133) Flory, P. J.; Semlyen, J. A. *J. Am. Chem. Soc.* **1966**, *88*, 3209.